Chemistry Europe
European Chemical Societies Publishing

WILEY VCH

Excellence in Chemistry Research

Announcing our new flagship journal

- Gold Open Access
- Publishing charges waived
- Preprints welcome
- Edited by active scientists

Meet the Editors of *ChemistryEurope*

Luisa De Cola
Università degli Studi di Milano Statale, Italy

Ive Hermans
University of Wisconsin-Madison, USA

Ken Tanaka
Tokyo Institute of Technology, Japan

Amyloid-β Peptides

Impact of N-Truncated Aβ Peptides on Cu- and Cu(Aβ)-Generated ROS: Cu^{I} Matters!

Charlène Esmieu,*[a] Guillaume Ferrand,[a, b] Valentina Borghesani,[a, b, c] and Christelle Hureau*[a, b]

Abstract: In vitro Cu($A\beta_{1-x}$)-induced ROS production has been extensively studied. Conversely, the ability of *N*-truncated isoforms of Aβ to alter the Cu-induced ROS production has been overlooked, even though they are main constituents of amyloid plaques found in the human brain. *N*-Truncated peptides at the positions 4 and 11 ($A\beta_{4-x}$ and $A\beta_{11-x}$) contain an amino-terminal copper and nickel (ATCUN) binding motif (H_2N-Xxx-Zzz-His) that confer them different coordination sites and higher affinities for Cu^{II} compared to the $A\beta_{1-x}$ peptide. It has further been proposed that the role of $A\beta_{4-x}$ peptide is to quench Cu^{II} toxicity in the brain. However, the role of Cu^{I} coordination has not been investigated to date. In contrast to Cu^{II}, Cu^{I} coordination is expected to be the same for *N*-truncated and *N*-intact peptides. Herein, we report in-depth characterizations and ROS production studies of Cu (Cu^{I} and Cu^{II}) complexes of the $A\beta_{4-16}$ and $A\beta_{11-16}$ *N*-truncated peptides. Our findings show that the *N*-truncated peptides do produce ROS when Cu^{I} is present in the medium, albeit to a lesser extent than the unmodified counterpart. In addition, when used as competitor ligands (i.e., in the presence of $A\beta_{1-16}$), the *N*-truncated peptides are not able to fully preclude Cu($A\beta_{1-16}$)-induced ROS production.

Introduction

Alzheimer disease (AD) is the most common cause of dementia, affecting more than 30 million people in the world, and is characterized by a brain deterioration leading to problems with memory, behaviour, and thinking. According to the "amyloid cascade hypothesis" the formation of abnormal amyloid deposits composed of amyloid-β peptides (Aβ) occurs in AD brain in extracellular locations at early stages of the disorder.[1] Aggregation of Aβ is linked to an accumulation of the peptide induced by an imbalance between its clearance and its production. Aβ is a fragment of 40–42 amino acids derived from the proteolytic cleavage of the amyloid precursor protein (APP) by the β- and γ-secretases. Studies of the composition of the senile plaques, undertaken in the middle of the 1980s, showed a heterogeneity of Aβ sequences including the presence of the *N*-truncated isoform at position 4 ($A\beta_{4-x}$).[2] Since then, numerous studies have shown the presence of a large number of N-terminally altered isoforms as the $A\beta_{3-x}$ and $A\beta_{11-x}$.[3] *N*-Truncated Aβs are produced either from the proteolysis of the full length ($A\beta_{1-x}$), or by dedicated proteases that process directly the APP.[4] According to ref. [5], isolated plaques from sporadic AD people contain up to 18.6% of $A\beta_{11-42}$, a level comparable to that of the $A\beta_{1-42}$ isoform.[5] $A\beta_{11-42}$ exposes a glutamic acid residue, which allows the N-terminal cyclization of the peptide to its pyroglutamate derivative ($pEA\beta_{11-42}$). It has been proposed that $pEA\beta_{11-42}$ also forms slowly over time.[6] Both forms are found in the senile plaques and cerebrospinal fluid. Recently, the *N*-truncated isoforms have drawn much more attention because of their putative protective role against protective role against reactive oxygen species (ROS).[3b,7]

The full length Aβ ($A\beta_{1-x}$) possesses two main domains: the last amino acid residues are involved in aggregation processes, and the first fourteenth are responsible for the coordination of metal ions, mainly copper and zinc.[3d,8] Cu ion bound to Aβ is able to catalyse the production of ROS through successive stepwise reduction of dioxygen.[9] This ROS production is assumed to be part of the enhancement of the oxidative stress found in AD brain that drives the disease.[10] Copper coordination to $A\beta_{1-x}$ or its validated model $A\beta_{1-16}$ (sequence in Scheme 1) has been widely investigated.[10–11] The coordination sites of Cu^{I} and Cu^{II} to Aβ at near physiological pH are depicted in Scheme 1.[8] The Cu^{II} is coordinated within $A\beta_{1-16}$ by the N-terminal amine, the adjacent carbonyl group from the peptide backbone, and two imidazole rings from two among the three Histidine (His) side-chain in a square-planar geometry with a conditional affinity constant of 10^{10} M^{-1} at pH 7.4.[12] The N-terminal truncation of $A\beta_{1-x}$ at positions 4 and 11 releases a

[a] Dr. C. Esmieu, G. Ferrand, Dr. V. Borghesani, Dr. C. Hureau
CNRS, LCC (Laboratoire de Chimie de Coordination)
205 route de Narbonne,BP 44099 31077 Toulouse Cedex 4 (France)
E-mail: charlene.esmieu@lcc-toulouse.fr
christelle.hureau@lcc-toulouse.fr
[b] G. Ferrand, Dr. V. Borghesani, Dr. C. Hureau
UPS, INPT, University of Toulouse, 31077 Toulouse Cedex 4 (France)
[c] Dr. V. Borghesani
current address: School of Chemistry
University of Birmingham, Edgbaston, B15 2TT (UK)
Supporting information and the ORCID identification number(s) for the author(s) of this article can be found under:
https://doi.org/10.1002/chem.202003949.

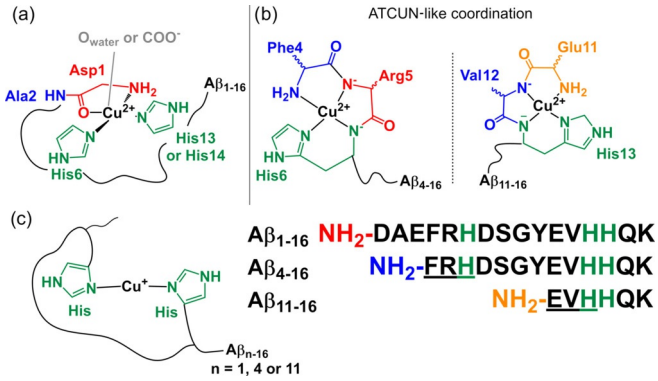

Scheme 1. Representation of the main coordination site of Cu^{II} bound to a) $A\beta_{1-16}$, b) $A\beta_{4-16}$ and $A\beta_{11-16}$, c) shared Cu^{I} coordination site at physiological pH and sequence of the Aβ peptides under investigation in the paper with the His in green and the ATCUN motif underlined.

peptide containing an amino-terminal copper and nickel motif (ATCUN, NH_2-Xxx-Zzz-His) that is known to bind Cu^{II} with high affinity constant (ca. 10^{14} M^{-1}).[13] The binding site of $A\beta_{4/11-16}$ (sequences in Scheme 1) is constituted by the N-terminal amine, the proximal (δ) nitrogen atom of the His side chain and both deprotonated amides of the peptide backbone in between the N-terminal amine and the His (Scheme 1).[13–14]

In contrast, the Cu^{I} coordination site is expected to be similar for the three peptides ($A\beta_{1/4/11-16}$) since the two imidazole rings required for Cu^{I} binding are present in the three sequences. It is thus anticipated that Cu^{I} lies in a diagonal environment made by two imidazole groups from the His residues at positions 6, 13 and 14 (13 and 14 only for the $A\beta_{11-16}$).[15] The affinity is also expected to be similar between the three peptides, while the values reported for $A\beta_{1-16}$ range between 10^{7} to 10^{10} M^{-1}.[15a,16]

A vast number of in vitro investigations on the production of ROS by the full length $A\beta_{1-40/42}$ or its C-terminally truncated model $A\beta_{1-16}$ in presence of Cu ions have been performed.[9] Importantly, evidences obtained by electrochemical studies indicated that direct electron transfer between $Cu^{I}(A\beta_{1-16})$ and $Cu^{II}(A\beta_{1-16})$ is hampered by a large reorganization energy and thus the reduction–oxidation proceed via an unusual mechanism.[9a] ROS are therefore produced by an "in between" state (IBS) in equilibrium with the $Cu^{I}(A\beta_{1-16})$ and $Cu^{II}(A\beta_{1-16})$. Structurally, it has been proposed that the Cu in the IBS is linked to the N-terminal amine, the carboxylate group from Asp1, and one imidazole group from one His of the peptide,[9e,17] but this model is still under discussion.[18]

Conversely, research on the ability of N-terminally truncated $Cu(A\beta_{4-16})$ to produce ROS are only very recent (and limited to studies with Cu^{II} only).[7a,13a,19] It has been shown that $A\beta_{4-16}$ presents a highly ordered ATCUN metal-binding site of low redox activity in the presence of Cu^{II} and ascorbate.[13a] Additionally it has been suggested that it can extract Cu^{II} from $Cu^{II}(A\beta_{1-16})$ and could have a crucial role in metal homeostasis[7a,20] and thus could be beneficial in the context of AD as an intrinsic competitor to prevent the ROS production generated by the Cu-metallated $A\beta_{1-x}$.[7a,c]

To gain a better understanding of the coordination chemistry of *N*-truncated peptides containing a ATCUN motif involved in AD, we have investigated the Cu^{II} and Cu^{I} binding properties of the $A\beta_{4-16}$ and $A\beta_{11-16}$ isoforms, and compared them to those of $A\beta_{1-16}$. Furthermore, we have challenged the ROS production ability of these two $Cu(A\beta_{4/11-16})$ in a more biologically relevant medium containing Cu^{I}. Finally, we further studied the ability of the *N*-truncated isoforms $A\beta_{4/11-16}$ to extract Cu^{I} and Cu^{II} from the $A\beta_{1-16}$ peptide and to impact the ROS production by $Cu(A\beta_{1-16})$. We confirm that $A\beta_{4-16}$ and $A\beta_{11-16}$ are both able to form redox-inert Cu^{II} complexes and can extract Cu^{II} from $Cu(A\beta_{1-16})$. However, and more importantly, we demonstrate that the high-affinity and redox-inert Cu^{II} ATCUN binding site of the *N*-truncated peptides is not enough to preclude ROS production. We show that this is due to 1) the capability of the peptides to bind Cu^{I} and 2) kinetically competitive processes (formation of the ATCUN Cu^{II} site versus reduction of Cu^{II}-bound to $A\beta_{4/11-16}$ in another site than the ATCUN one). In addition, when $A\beta_{4/11-16}$ are regarded as intrinsic redox-silencing chelators, their effect on ROS production is dependent on the starting conditions, and again when Cu^{I} is present in the medium, ROS production is only moderately reduced, in line with similar Cu^{I} affinity of the *N*-truncated peptides versus the unmodified counterpart. As a result, a biologically relevant mixture of the various Cu(peptides) species can produce ROS in the presence of Cu^{I}, dioxygen and ascorbate, which mirror physiological conditions.

Results and Discussion

Characterization of $Cu(A\beta_{4-16})$ and $Cu(A\beta_{11-16})$

Cu^{II} binding kinetics

Stopped-flow measurements were conducted to qualitatively evaluate the kinetics of Cu^{II} coordination by the two *N*-truncated peptides (Figure S1). The stopped-flow system used was coupled to a diode array detector recording in the 250–720 nm range, allowing the d-d band increase (for the $Cu^{II}(A\beta_{4/11-16})_{ATCUN}$ complexes, $\lambda_{max}=520$ nm), linked to the formation of the Cu^{II} complexes, to be monitored over time. In a quasi-stoichiometric amount of Cu^{II} (0.9 equiv per peptide) and at about 0.5 mM, $A\beta_{11-16}$ is faster in coordinating Cu^{II} than $A\beta_{4-16}$, with $t_{1/2}=0.13\pm0.02$ s vs. $t_{1/2}=0.45\pm0.1$ s for $A\beta_{11-16}$ and $A\beta_{4-16}$, respectively. The value found for $A\beta_{4-16}$ agrees fairly well with that recently determined by competition and double mixing stopped-flow experiments and attributed to the formation of the $Cu^{II}(A\beta_{4-16})_{ATCUN}$ motif once the Cu^{II} is anchored to the peptide.[21] Additionally, the value found for $Cu^{II}(A\beta_{11-16})$ is consistent with the value very recently determined[22] for the short GGH peptide by classical stopped-flow experiments and attributed to the reshuffling of the Cu^{II} site forming the ATCUN motif after initial anchoring to the N-terminal and side-chain of His groups. In addition, it was not possible to measure the rate of Cu^{II} binding to $A\beta_{1-16}$ under the very same conditions, thus indicating that Cu^{II} anchoring to the peptide (mainly via His or carboxylate containing amino-acid residues),[11c] is much faster (Figure S1). This confirms that the rate determined with the

Table 1. Apparent binding affinities determined for Cu^{I}, conditional binding affinities reported for Cu^{II}, redox potentials, UV/Vis and EPR parameters determined for $^{65}Cu(II)$ for $A\beta_{4-16}$ and $A\beta_{11-16}$ peptides.

Peptide	$^{a}K_a$ [μM^{-1}] pCu for Cu^{I}[a]	$^{c}K_a$ [M^{-1}] pCu for Cu^{II}[a]	EP (vs. NHE) [V]			UV/Vis	EPR (A in G)[b]		
			$Cu^{2+}\rightarrow Cu^{+}$	$Cu^{+}\rightarrow Cu^{2+}$	$Cu^{2+}\rightarrow Cu^{3+}$	λ_{max} [nm] (ε in $M^{-1}cm^{-1}$)	$g_{\perp}$	$g_{\parallel}$	$A_{\parallel}$
$A\beta_{4-16}$	3.7 ± 0.4 5.9	$\approx10^{13}$ 12.8[13a]	−1.30	0.48	1.05	520 (100)	2.055	2.18	211
$A\beta_{11-16}$	1.9 ± 0.5 5.6	$\approx10^{13}$ 12.8[13b]	−1.50	0.51	1.02	522 (102)	2.049	2.19	217
$A\beta_{1-16}$	7.5 ± 1.0 6.2	$\approx10^{10}$ 8.9[12a]				625 (65)	2.06	2.27	181

[a] $pCu=-\log[Cu]_{free}$ for $1.2\times[Cu]=[L]$ and $[Cu]=10\ \mu M$. [b] EPR parameters were determined in 50 mM HEPES (pH 7.4) buffer containing 10% glycerol (v/v).

$A\beta_{11-16}$ and $A\beta_{4-16}$ mainly attests to the formation of the ATCUN site around the Cu^{II} ion.

The difference observed between the two peptides (formation of $Cu^{II}(A\beta_{4-16})_{ATCUN}$ about three times slower than that of $Cu^{II}(A\beta_{11-16})_{ATCUN}$) may be linked to the presence of His13 and His14. Such a His dyad creates a second independent and thus competing site in $A\beta_{4-16}$, as recently observed for similar peptides encompassing both a ATCUN and a His dyad site.[23] Conversely, the His dyad belongs to the ATCUN motif in $A\beta_{11-16}$, thus helping the anchoring of Cu^{II} near the final ATCUN site.

Briefly, the values we determined here mainly mirror the time required to accommodate the Cu^{II} in the ATCUN site, in line with a very fast anchoring process (thus not rate-limiting) at such high concentration.

Electron paramagnetic resonance

Both complexes $Cu^{II}(A\beta_{4-16})$ and $Cu^{II}(A\beta_{11-16})$ display a classical EPR signal for a 4N coordination, with superhyperfine lines in the perpendicular region indicative of N equatorial ligands (Figure S2 (b) and (d)) and reminiscent of Cu^{II} bound in a ATCUN[7b,24] motif including those obtained with $A\beta_{11-15}$ and $A\beta_{4-16}$.[13,14,25] This signature strongly differs from that of $Cu^{II}(A\beta_{1-16})$ (Figure S2 (a)), allowing the removal of Cu^{II} from $Cu^{II}(A\beta_{1-16})$ by the two *N*-truncated peptides to be easily monitored. EPR signatures were identical with or without $A\beta_{1-16}$, demonstrating that the final species formed in the presence of an equimolar mixture of $A\beta_{4/11-16}$ and $A\beta_{1-16}$ is the $Cu^{II}(A\beta_{4/11-16})_{ATCUN}$ complex (Figure S2 (c) and (e)). The EPR parameters are summarized in Table 1.

Electrochemistry

The cyclic voltammograms (CV) of Cu bound to $Cu^{II}(A\beta_{4-16})$ and $Cu^{II}(A\beta_{11-16})$ are shown in Figure 1 and Figure S3. The $A\beta_{4-16}$ peptide alone displays an irreversible oxidation at $E^{pa}=0.76$ V vs. SCE (1.00 V vs. NHE) corresponding to Tyr10 oxidation (Figure S3).[13a,26] The $Cu^{II}(A\beta_{4-16})$ complex shows an irreversible anodic process at $E^{pa}=0.81$ V vs. SCE (1.05 V vs. NHE). This potential is close to the previously reported value for the oxidation of Cu^{II} to Cu^{III} in an ATCUN motif.[13a,27] The unusual intensity of this peak originated from the addition of the two processes mentioned before (i.e., Tyr10 and Cu^{II} to Cu^{III} oxidations). The $Cu^{II}(A\beta_{4-16})$ complex is reduced at $E^{pc}=-1.06$ V vs. SCE (−1.30 V vs. NHE), leading to $Cu^{I}(A\beta_{4-16})^{*}$ species that chemically evolves toward the stable $Cu^{I}(A\beta_{4-16})_{L}$ species that is reoxidized at $E^{pa}=0.24$ V vs. SCE (0.48 V vs. NHE). It can be postulated that the Cu^{II} coordination changes upon reduction from a typical 4N coordination by the ATCUN motif to a linear coordination between to imidazole rings of the His residues to accommodate the Cu^{I} ion. The oxidation pattern is indeed strongly reminiscent of the oxidation of a His-Cu^{I}-His species.[28]

The $A\beta_{11-16}$ peptide alone yield no electrochemical activity, in line with the absence of a redox-active amino acid residue (i.e., Tyr10) in the peptide sequence (Figure S3). As for the $Cu^{II}(A\beta_{4-}$

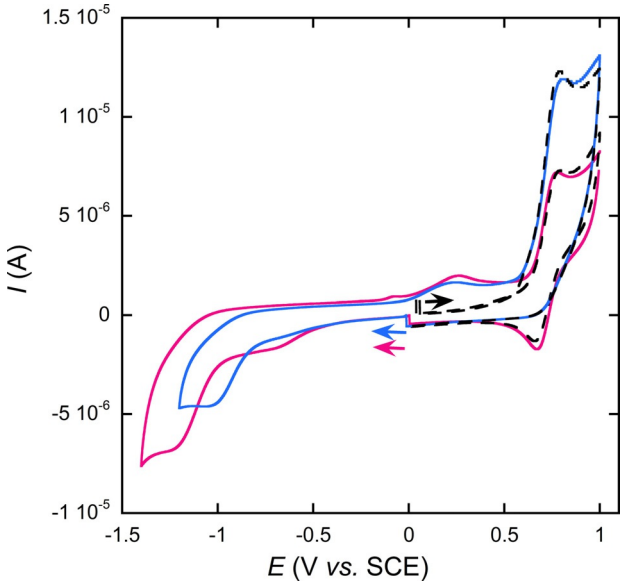

Figure 1. Cyclic voltammogram (CV) of $Cu^{II}(A\beta_{11-16})$ (pink line) and $Cu^{II}(A\beta_{4-16})$ (blue line). The dotted black lines are CV measured in oxidation showing no electrochemical process at 0.24 V vs. SCE. $[A\beta_{4/11-16}]=0.5$ mM, $[Cu^{II}]=0.48$ mM in [phosphate buffer] = 50 mM at pH 7.4 under argon. Scan rate = 100 mV $s^{-1;}$ WE = Glassy carbon, Ref = SCE, CE = Pt wire. First scans are shown starting from the open circuit potential (from the arrows).

$_{16}$), the $Cu^{II}(A\beta_{11-16})$ can be oxidized to $Cu^{III}(A\beta_{11-16})$ at $E^{pa}=$ 0.78 V vs. SCE (1.02 V vs. NHE) but this time the Cu^{III} species can be reduced at $E^{pa}=0.67$ V vs. SCE (0.91 V vs. NHE) leading to a quasi-reversible process. The reversibility of the Cu(III/II) process in the ATCUN motif is dependent on the nature of the Xxx and Zzz amino acid residues, which can explain the difference with $Cu^{II}(A\beta_{4-16})$ in addition to the absence of the concomitant oxidation of Tyr10.[7b,29] $Cu^{II}(A\beta_{11-16})$ shows an irreversible cathodic peak at $E^{pc}=-1.26$ V vs. SCE (−1.50 V vs. NHE) attributed to its reduction followed by a structural rearrangement leading to a re-oxidation peak at $E^{pa}=0.27$ V vs. SCE (0.51 V vs. NHE), as observed for $Cu^{II}(A\beta_{4-16})$. The different cathodic potentials between the two complexes can be tentatively attributed to 1) a less stabilized ATCUN motif in the $Cu^{II}(A\beta_{4-16})$ due to the presence of Arg5 adjacent to His6; such proximity between these two amino-acid residues has been previously proposed to hinder the Cu^{II} binding by His,[30] and 2) more stable Cu^{I} species due to the presence of three His leading to three possible His binding dyads. Conversely, the re-oxidation peak of the electrochemically generated Cu^{I} species are at the same potential value, in line with similar Cu^{I} coordination. To summarize, we have thus observed a classical electrochemical-chemical-electrochemical-chemical (ECEC) mechanism, in which the first electrochemical process is the reduction of the Cu^{II} in the ATCUN site, the first chemical evolution leads to a linearly bound bis-His Cu^{I} species that is oxidized (second electrochemical process) and evolves back to the initial Cu^{II} species.

For both *N*-truncated sequences, the Cu^{II} complexes can be reduced to Cu^{I} but at a very low potential, $E^{pc}<-1$ V vs. SCE. This reduction potential of the Cu^{II} complexes is well beyond the oxidation potential of ascorbate; hence, the Cu^{II} complexes are expected to be stable upon reduction with ascorbate.[31] Electrochemical potential (EP) are summarized in Table 1.

Cu^{I} NMR spectroscopic analysis

NMR experiments were performed to evaluate the Cu^{I} binding to the different peptides. Expected chemical shifts of the protons in the Cu^{I} vicinity are observed for $Cu^{I}(A\beta_{1-16})$ complex. For instance, in the aromatic region, the H_δ and $H\varepsilon$ protons of His, present at around 7.70 and 6.85 ppm, are strongly shifted, indicating that the His residue are involved in Cu^{I} binding (Figure 2a).[9b] Similar trends are followed by the two *N*-truncated peptides, with a large shift of the protons of the His residues. Interestingly the protons of Val12 are strongly shifted for the $A\beta_{11-16}$ peptide but are not really affected in the $A\beta_{1-16}$ and $A\beta_{4-16}$ cases. This is strongly indicative that the coordination of Cu^{I} into the $A\beta_{11-16}$ differs from that in $A\beta_{1-16}$ and $A\beta_{4-16}$. From a peptide sequence point of view, $A\beta_{11-16}$ lacks the His6, implying that the Cu^{I} is coordinated only by the His 13 and His 14. The different proton behaviour of Val12 observed for $A\beta_{11-16}$ suggests the involvement of the His6 in the Cu^{I} coordination with the $A\beta_{1-16}$ and $A\beta_{4-16}$ peptides, in contrast to our previous report.[9b] The present observation is consistent with a recently published article showing that His6 is the His mainly involved in Cu^{I} binding.[15a]

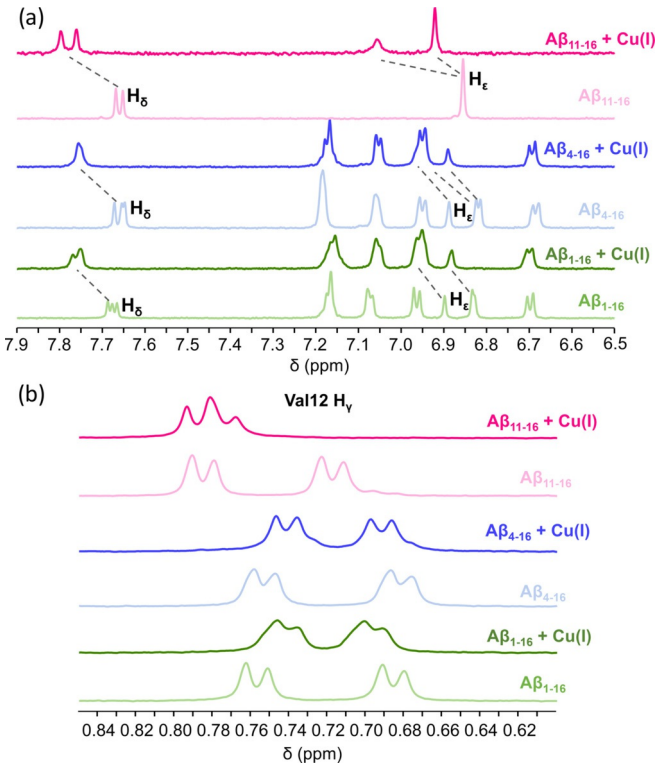

Figure 2. ^{1}H NMR spectra of $A\beta_{1-16}$ (light green) with 1 equivalent of Cu^{I} (dark green), of $A\beta_{4-16}$ (light blue) with 1 equivalent of Cu^{I} (dark blue), and of $A\beta_{11-16}$ (light pink) with 1 equivalent of Cu^{I} (dark pink) at pH 7.3 in phosphate buffer (200 mM), His region (a) and Val12 region (b). The chemical shifts of His protons observed upon addition of Cu^{I} are indicated with dotted lines.

Affinity of $A\beta_{1/4/11-16}$ for Cu^{I}

Cu^{I} apparent binding affinity to $A\beta_{1/4/11-16}$ were determined by competition with the chromophoric $[Cu^{I}(Fz)_2]^{3-}$ (Fz = ferrozine = 5,6-diphenyl-3-(2-pyridyl)-1,2,4-tri-azine-4,4′′-disulfonic acid) according to the model of Alies et al. (Table 1 and Figure S4).[16b] This gives K_a values of $1.9\pm0.5\ 10^6\ M^{-1}$ and $3.7\pm0.4\ 10^6\ M^{-1}$ for $Cu^{I}(A\beta_{11-16})$ and $Cu^{I}(A\beta_{4-16})$, respectively. Those values are of the same order of magnitude as that reported by Alies et al. for the $Cu^{I}(A\beta_{1-16})$ complex ($7.5\pm1.0\ 10^6\ M^{-1}$) determined by the same method. The two *N*-truncated peptides studied here are His-containing peptide sequences. It is then anticipated that $A\beta_{4/11-16}$ binds to soft Cu^{I} cation similarly to the $A\beta_{1-16}$ with two His in a linear geometry. The lower value found for $A\beta_{11-16}$ can be attributed to the lack of the third His (His6), in line with the weaker value reported for the mutated $A\beta_{1-16}$-H6A peptide.[16a,b] The two-fold weaker affinity for the 3-His containing $A\beta_{4-16}$ peptide may mirror second sphere effects due to modification of the N-terminal sequence, and is in line with modification of the Cu^{I} affinity by acetylation of the terminal amine, as previously reported.[16b]

We have described here the Cu^{II} and Cu^{I} coordination sites in the three peptides under study (Scheme 1) and also determined their Cu^{I} affinity values (Table 1). From those values and the similarity of binding sites, it is expected that the *N*-truncated peptides can compete with $A\beta_{1-16}$ peptide for Cu^{I} coordina-

tion, but cannot fully remove Cu^{I} from $Cu^{I}A\beta_{1-16}$. In contrast, the ATCUN peptides do remove Cu^{II} from $Cu^{II}A\beta_{1-16}$.

Reactive oxygen species (ROS) production

The intrinsic properties of Cu bound to the *N*-truncated Aβ to produce ROS in the presence of ascorbate and O_2 were evaluated according to routine methods.[32] Briefly, to evaluate the ability of Cu to produce ROS when this latter is bound to the different peptides, an ascorbate consumption assay was performed in the presence of the different Aβ peptides, oxygen, and a slightly substoichiometric amount of Cu^{II} (for details see the Supporting Information).[31,33] The concentration of ascorbate that fuels the reaction was followed by UV/Vis at 265 nm.

Starting from Cu^{II}

Compared to the $A\beta_{1-16}$ which produces a high level of ROS in these conditions, indicated by a rapid and complete consumption of the ascorbate in 2000 s (33 min), $A\beta_{4/11-16}$ prevents the formation of ROS (Figure S5). Between 2500 and 3000 s of the experiment, a rate constant for the ascorbate consumption around 0.04 ms^{-1} is calculated (Figure 4a, left). This basal consumption of ascorbate is attributed to the auto-oxidation of ascorbate under our experimental conditions; indeed, the same value is obtained with ascorbate only in the buffer (Figure S5). These results show the ability of both *N*-truncated peptides to chelate Cu^{II} in the ATCUN motif, stabilizing the Cu^{II} redox state in the $Cu^{II}(A\beta_{4/11-16})_{ATCUN}$ complex and is in line with the low reduction potential of the Cu(II/I) couple observed by voltammetry. Those results are also consistent with the reported lower level of hydroxyl radical produced with $Cu^{II}(A\beta_{4-16})_{ATCUN}$ measured by APF (2-[6-(4′-amino)phenoxy-3*H*-xanthen-3-on-9-yl]-benzoic acid) fluorescence under similar concentration conditions.[13a]

Starting from Cu(II/I)

To go further and challenge the ability of $A\beta_{4/11-16}$ to stop ROS under more biologically relevant conditions, the ascorbate consumption assay was performed in the presence of Cu^{I} and in the presence of a mixture of Cu^{I} and Cu^{II}. Such conditions could better mimic the extracellular brain environment, which is, at the same time rich in ascorbate and dioxygen and where the predominant redox state of Cu is not determined.[34]

To obtain the Cu(II/I) mixture, Cu^{II} was first reacted with ascorbate to generate Cu^{I} by redox cycling and then the different Aβ peptide forms (i.e., $A\beta_{1-16}$, $A\beta_{4-16}$ and $A\beta_{11-16}$) were added (Figure 3).

Overall, the trend of the ascorbate consumption reflecting the ROS production is close to that reported with Cu^{II} only (Figure 3, Figure 4b, left). Both *N*-truncated peptides can reduce the consumption of ascorbate significantly compared to the non-truncated peptide $A\beta_{1-16}$. For $A\beta_{4/11-16}$, after 1500 s of reaction, the rate constant for the consumption of ascorbate are comparable with that obtained with Cu^{II} only, irrespective of the initial presence of Cu^{I} (Figure 4d, right). This observation

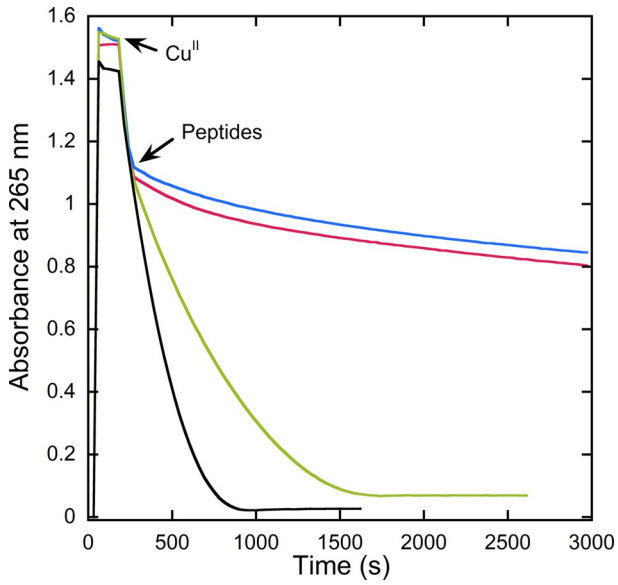

Figure 3. Kinetics of ascorbate consumption, followed by UV/Vis spectroscopy at 265 nm. Asc + Cu^{II} (black curve), Asc + Cu^{II} + $A\beta_{1-16}$ (green curve), Asc + Cu^{II} + $A\beta_{11-16}$ (pink curve), Asc + Cu^{II} + $A\beta_{4-16}$ (blue curve). [$A\beta_{1/4/11-16}$] = 12 μM, [Cu^{II}] = 10 μM, [Asc] = 100 μM, [HEPES] = 100 mM, pH 7.4.

indicates that, at the end of the kinetic study, the $Cu^{II}(A\beta_{4/11-16})_{ATCUN}$ complexes are the predominant species in solution. Hence, we propose that the Cu^{I} initially present has been oxidized in Cu^{II}, mainly generating the redox stable Cu^{II} complexes as seen before.

However, the initial rates of the ascorbate consumption (between 260 and 900 s) are accentuated in the presence of Cu^{I} (Figure 4d, left) compared to experiments done starting with Cu^{II} only (Figure 4a). Quantitatively, in presence of Cu^{I}, the initial ascorbate consumption rate constants are four times higher (0.05 ms^{-1} vs. 0.21 ms^{-1} for $A\beta_{4-16}$ and 0.07 ms^{-1} vs. 0.28 ms^{-1} for $A\beta_{11-16}$). We hypothesized that a linear $Cu^{I}(A\beta_{4/11-16})$ complex is initially generated by the direct coordination of Cu^{I} by the peptides and are oxidized by O_2, giving a Cu^{II} species that may keep a linear coordination mode (Scheme 2). This new intermediate species, named $Cu^{II}(A\beta_{4/11-16})_{L}$ (L for linear) can evolve in two different ways: 1) through a rearrangement to form the redox stable $Cu^{II}(A\beta_{4/11-16})_{ATCUN}$ (Scheme 2, black arrow), or 2) can be reduced by ascorbate and thus produce ROS by redox cycling (Scheme 2, grey arrow). Therefore, the ROS production becomes dependent on the kinetics of the reduction of the transient $Cu^{II}(A\beta_{4/11-16})_{L}$ species versus its rearrangement into the $Cu^{II}(A\beta_{4/11-16})_{ATCUN}$ complex.

Scheme 2. Schematic representation of the formation of the transient $Cu^{II}(A\beta_{4/11-16})_{L}$ by oxidation of the $Cu^{I}(A\beta_{4/11-16})$ leading to either its re-organization into $Cu^{II}(A\beta_{4/11-16})_{ATCUN}$ (black arrow) or to its reduction (grey arrow).

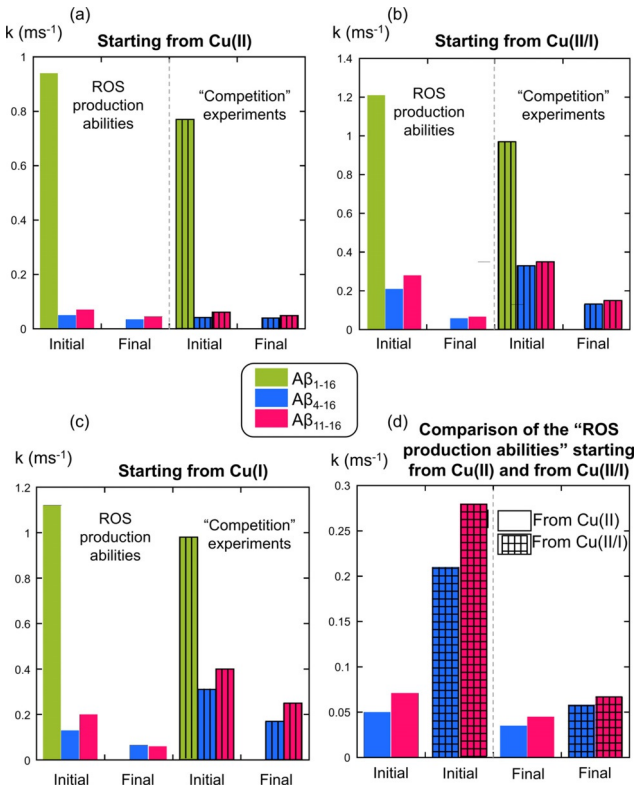

Figure 4. Rate constant of the ascorbate consumption of each experiment calculated at the beginning of the kinetics, during the first 5 minutes after the addition of the peptides (initial) and at the end during the 8 last minutes of the kinetics (final). (Panel a) Starting from Cu^{II}; (Panel b) starting from Cu(II/I); (Panel c) starting from Cu^{I} and (Panel d) comparison between Panel a and Panel b. Rate constants are calculated on at least three independent experiments with a good reproducibility for each condition, the mean values are plotted. On Panels a, b and c the vertical striped bars represent experiments done with the *N*-truncated peptides used as competitor compounds to extract Cu from $Cu(A\beta_{1-16})$. In Panel d the grid bars represent experiments starting from Cu(II/I). $[A\beta_{1/4/11-16}] = 12\ \mu M$, $[Cu^{II}] = 10\ \mu M$, [Asc] = 100 μM, [HEPES] = 100 mM, pH 7.4.

In the presence of more peptide (2 equiv, see Figure S6), the rate of ascorbate consumption is slower for all three peptides, in line with the previous report on $A\beta_{1-16}$,[17] and shows a decrease in the amount of free Cu.

Starting from Cu^{I} only

In this experiment the Cu^{I} was generated in situ directly in the sealed UV/Vis cuvette by addition of ascorbate to a Cu^{II} solution under anaerobic conditions. The different peptides were then added to the Cu^{I}-asc solution to form the $Cu^{I}(A\beta_{1/4//11-16})$ species. The cuvette was finally opened at 1120 s and air was vigorously bubbled inside. The ascorbate consumption exhibited the same shape whether starting from Cu^{I} or from the mixture of Cu(II/I) (Figure S7). The production of ROS was quicker at the beginning and progressively stabilized to meet the level attributed to the auto-oxidation of the ascorbate, meaning a total arrest of the ROS production by the $A\beta_{4/11-16}$ peptides (Figure 4c, left). Again we attribute this phenomenon to the oxidation of the $Cu^{I}(A\beta_{4/11-16})_{L}$, leading to a Cu^{II} species that can be reduced by ascorbate or undergo a rearrangement to form the redox inert $Cu^{II}(A\beta_{4/11-16})_{ATCUN}$ complex (Scheme 2).

Ability of the *N*-truncated peptides to extract Cu^{II} and Cu^{I} from $A\beta_{1-16}$ peptide: Competition experiments

ROS from Cu^{II}

As the *N*-truncated forms of the peptide (i.e., $A\beta_{4-16}$ and $A\beta_{11-16}$) co-exist with non *N*-truncated forms (i.e., $A\beta_{1-16}$) in the brain,[3a–c,5] the effect on ROS production of having the two types of peptide in the experiments (i.e., *N*-truncated and non-truncated) has been investigated. An ascorbate consumption assay was performed in the presence of O_2 and an equimolar mixture of peptides $A\beta_{1-16}$ and $A\beta_{4-16}$ or peptides $A\beta_{1-16}$ and $A\beta_{11-16}$, and a slightly substoichiometric amount of Cu^{II} (Figure S8). In the presence of $A\beta_{4-16}$ or $A\beta_{11-16}$ and $Cu^{II}(A\beta_{1-16})$ the ascorbate consumption resembles that of $Cu^{II}(A\beta_{4/11-16})$ (Figure 4a, right). The formation of the thermodynamically stable $Cu^{II}(A\beta_{4/11-16})_{ATCUN}$, in line with the EPR data showing the removal of Cu^{II} bound to $A\beta_{1-16}$ by the ATCUN-peptides, prevents the production of ROS.

Stopped-flow Cu^{II} exchange kinetics

The ability of the *N*-truncated peptides to extract Cu^{II} from $Cu^{II}(A\beta_{1-16})$ has been investigated by stopped-flow measurements at 0.5 mM working concentration. The total extraction of the Cu^{II} from the $A\beta_{1-16}$ is slow and takes about 60 s for both *N*-truncated peptides (Figure S9) with $A\beta_{4-16}$ faster than $A\beta_{11-16}$ in extracting Cu^{II} ($t_{1/2}$ ca. 15.5 s vs. $t_{1/2}$ ca. 10.8 s for $A\beta_{11-16}$ and $A\beta_{4-16}$ respectively).

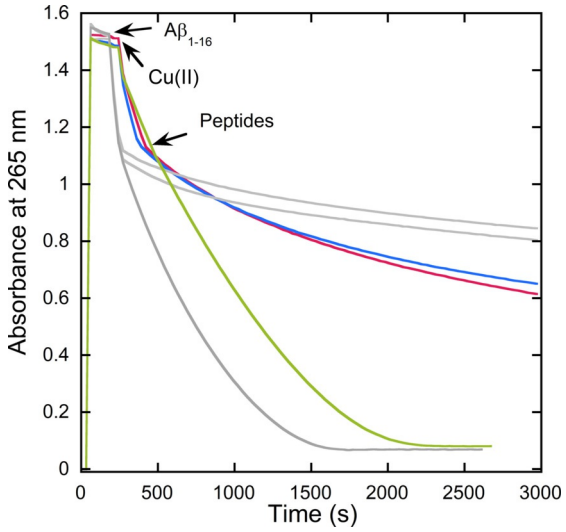

Figure 5. Kinetics of ascorbate consumption, followed by UV/Vis spectroscopy at 265 nm. Asc + $A\beta_{1-16}$ + Cu^{II} + either $A\beta_{1-16}$ (green curve), or + $A\beta_{11-16}$ (pink curve), or + $A\beta_{4-16}$ (blue curve). The arrows indicate the order and time of the different addition into the UV/Vis cuvette. $[A\beta_{1/4/11-16}] = 12\ \mu M$ or 24 μM (green curve), $[Cu^{II}] = 10\ \mu M$, [Asc] = 100 μM, [HEPES] = 100 mM, pH 7.4. The grey lines are the data presented in Figure 3 (Cu(II/I) + peptides), for comparison.

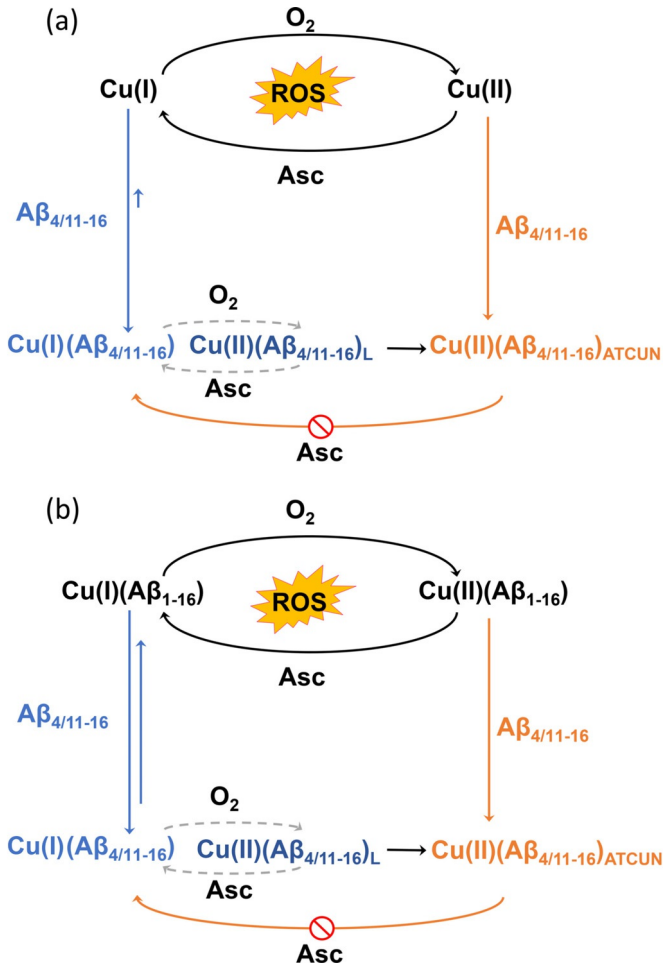

Scheme 3. Summary of Cu chelation and ROS production by the *N*-truncated peptides in absence (a) or in presence of $A\beta_{1-16}$ (b). The orange part represent the coordination of Cu^{II} leading to the formation of an $Cu^{II}(A\beta_{4/11-16})_{ATCUN}$ complex inert toward ascorbate reduction. The blue part represents the Cu^{I} coordination generating a Cu^{I} complex, which can be oxidized by O_2 to a transient species $Cu^{II}(A\beta_{4/11-16})_L$ where the Cu^{II} is still bound linearly (dark blue). $Cu^{II}(A\beta_{4/11-16})_L$ can be reduced with ascorbate and generate ROS (dashed grey arrow) or can undergo rearrangement to form the redox inert $Cu^{II}(A\beta_{4/11-16})_{ATCUN}$ complex (full black arrow). In the presence of $A\beta_{1-16}$ the Cu^{I} is in equilibrium between the *N*-truncated forms and the $A\beta_{1-16}$ causing the production of more ROS.

ROS from Cu(II/I)

As previously described, ROS production measurement was also conducted in the presence of $Cu(A\beta_{1-16})$ in its two redox forms. The experiment involved adding ascorbate to pre-form the $Cu^{II}(A\beta_{1-16})$ complex, and then adding the *N*-truncated peptides during ascorbate consumption (Figure 5, blue and pink curves).

The Cu induced ROS level increased in the presence of $A\beta_{1-16}$ for both *N*-truncated peptides (compared Figure 3 vs. Figure 5, and see Figure 4b, right). In other terms, the presence of $A\beta_{1-16}$ in the reaction medium slows down the formation of the redox stable $Cu^{II}(A\beta_{4/11-16})_{ATCUN}$ complex. As was previously demonstrated (Table 1), the $A\beta_{1-16}$ cannot compete with the *N*-truncated peptides for Cu^{II} coordination, the difference in the ROS production is then assigned to Cu^{I} complex formation, for which the $A\beta_{1-16}$ and the *N*-truncated peptides have the same affinity.

The existence of an equilibrium between the different Cu^{I} complexes (i.e., $Cu^{I}(A\beta_{4/11-16})$ and $Cu^{I}(A\beta_{1-16})$) would contribute to slow the formation of the redox stable $Cu^{II}(A\beta_{4/11-16})_{ATCUN}$ complexes and maintain the $Cu^{I}(A\beta_{1-16})$ species in solution, leading to a significant increase in ROS production (Scheme 3b).

An ascorbate consumption experiment was also performed by first adding the *N*-truncated peptides to the Cu(II/I) mixture, allowing the formation of the $Cu^{II}(A\beta_{4/11-16})$ and $Cu^{I}(A\beta_{4/11-16})$ species and followed by the addition of the $A\beta_{1-16}$ at 25 s (before the full formation of the $Cu^{II}(A\beta_{4/11-16})_{ATCUN}$, Figure S10). Again, the ROS production increases in the presence of $A\beta_{1-16}$, showing that the $Cu^{I}(A\beta_{1-16})$ complex, which produces ROS, can be quickly generated by exchange with the $Cu^{I}(A\beta_{4/11-16})$. The coordination and exchange processes are summarized in Scheme 3b.

ROS from Cu^{I}

As expected, when the same competition experiment was done in the presence of Cu^{I} alone, the results obtained were similar (Figure 4c, right and Figure S11).

Proposed mechanisms

Based on the previously described studies, we here propose two mechanisms to explain 1) the ROS production of $Cu(A\beta_{4/11-16})$ (Scheme 3a) and 2) the impact of $A\beta_{4/11-16}$ on the $Cu(A\beta_{1-16})$ ROS production (Scheme 3b).

1) In the presence of Cu^{II}, we observe the formation of $Cu^{II}(A\beta_{4/11-16})$ complexes that are resistant to ascorbate reduction (and thus there is no ROS produced), in contrast to $Cu(A\beta_{1-16})$ (orange arrow in Scheme 3a). In the presence of Cu^{I} or Cu(II/I), the ROS production ability of the peptides differs. For the $Cu(A\beta_{1-16})$, its ability to catalyse ROS formation has been widely studied before and is not dependent on the Cu redox starting state (See ref.[9]). For the *N*-truncated peptides, we thus anticipate that a key step in the mechanism is the formation of a $Cu^{II}(A\beta_{4/11-16})_L$ intermediate species that can evolve either i) back to the reduced counterpart (grey line in Scheme 2 and dotted grey line in Scheme 3a) or ii) to the $Cu^{II}(A\beta_{4/11-16})_{ATCUN}$ site (black line in Scheme 2 and Scheme 3a). To validate such hypothesis, Cu(II/I) ROS experiments were conducted with an higher ascorbate concentration, with the aim to favour the reduction of $Cu^{II}(A\beta_{4/11-16})_L$ (grey line in Scheme 2). It has to be noted that these conditions are probably closer to the AD brain environment, in which concentrations up to millimolar levels of ascorbate can be found.[35] At 500 μM of ascorbate $Cu(A\beta_{11-16})$ produces ROS as much as the parent $Cu(A\beta_{1-16})$, whereas the ROS production level of $Cu(A\beta_{4-16})$ is similar to that evaluated at 100 μM ascorbate (Figure S12). There are two possible explanations: i) the rate of the formation of the reduction-resistant $Cu^{II}(A\beta_{4/11-16})_{ATCUN}$ versus the rate of

the reduction of the $Cu^{II}(A\beta_{4/11-16})_L$ is faster for $A\beta_{4-16}$ than $A\beta_{11-16}$ or ii) the amount of free Cu^{I} contributing to the ROS produced is higher for $A\beta_{11-16}$, which has a weaker binding affinity (see Table 1). The identification of the Cu^{II} binding site in the $Cu^{II}(A\beta_{4/11-16})_L$ species is beyond the scope of the present report and is based on in-house experience of similar studies on the $Cu(A\beta_{1-16})$ complex (see refs.[9a,e,17,36]). However we can propose a linearly bound Cu^{II} species in which the Cu^{II} might be linked by two His (reminiscent from Cu^{I} site) or by one His and the N-terminal amine, based on recent articles aimed at deciphering the first species appearing during the formation of $Cu^{II}(A\beta_{4-16})_{ATCUN}$[21] and $Cu^{II}(GGH)_{ATCUN}$.[22]

2) In the presence of $Cu^{II}(A\beta_{1-16})$, the time required for Cu^{II} to become bound inside the *N*-truncated peptides is at least one order of magnitude longer than for Cu^{II} (compare Figures S1 and S8) and there is no ROS produced provided that the mixture time between $Cu^{II}(A\beta_{1-16})$ and the $A\beta_{4/11-16}$ is long enough. In the presence of $Cu^{II/I}(A\beta_{1-16})$, the main difference compared to Cu(II/I) is the almost equal distribution between $Cu^{I}(A\beta_{1-16})$ and $Cu^{I}(A\beta_{4-16})$ or $Cu^{I}(A\beta_{11-16})$ that decreases the amount of $Cu^{I}(A\beta_{4/11-16})$ present in the medium and thus the concentration of their oxidized counterparts. As a consequence, the formation of the $Cu^{II}(A\beta_{4/11-16})_{ATCUN}$ species is slowed down, allowing more ROS to be produced.

Conclusion

We have investigated the Cu^{II} and Cu^{I} binding properties of the *N*-truncated $A\beta_{11-16}$ and $A\beta_{4-16}$ peptide isoforms, and compared them to the $A\beta_{1-16}$. We show by EPR, electrochemistry and ascorbate consumption assays that $A\beta_{11-16}$ can form a redox-inert Cu^{II} complex and can extract Cu^{II} from the $Cu^{II}(A\beta_{1-16})$ as can its analogue $A\beta_{4-16}$ that was previously studied. However, we demonstrate that the presence of the ATCUN motif into the *N*-truncated peptides that present high affinity constant for Cu^{II} does not guaranty its redox inertness in the presence of Cu^{I}. We then show that a key factor is the ratio between 1) the rate of reorganization of the intermediate $Cu^{II}(A\beta_{4/11-16})_L$ species into the $Cu^{II}(A\beta_{4/11-16})_{ATCUN}$ complex and 2) the rate of its reduction to $Cu^{I}(A\beta_{4/11-16})$. Such ratio is different for both *N*-truncated peptides, with only the $A\beta_{4-16}$ being able to form the reduction-resistant ATCUN complex even at high ascorbate concentration. Hence, we can foresee that in biologically relevant conditions, the $A\beta_{4-16}$ does not participate in ROS formation, in contrast to the other two peptides.

The in situ formation of ATCUN binding motifs by dedicated proteases has been reported as a possible pro-drug approach,[37] although it requires a peptide sequence suitable for going through the blood–brain barrier. Along a similar research line, other ATCUN peptides have also been studied.[38] Following a similar line of though, it could be anticipated that $A\beta_{4-16}$ could play a similar role, as a natural peptide drug, which would counterbalance the ROS produced by $Cu(A\beta_{1-16})$ by extracting Cu^{II} and redox-silencing it. If one considers only the Cu^{II} state, $A\beta_{4-16}$ is indeed able to extract it from $Cu(A\beta_{1-16})$ and further redox-silence it, thus preventing ROS formation by $Cu(A\beta_{1-16})$. However in the presence of Cu^{I}, which is likely the most biologically relevant situation, the $A\beta_{4-16}$ is only able to reduce the ROS production of $Cu(A\beta_{1-16})$ but cannot fully preclude it as other synthetic molecules do.[39] This points out the importance of considering Cu^{I} not only in the metal homeostasis in the synaptic cleft but also in the design of drug candidates.

Experimental Section

All chemicals were purchased from Sigma–Aldrich or TCI chemicals. The solutions were prepared in milliQ water (resistance: 18.2 MΩ.cm) except when noted. Cu^{II} solutions were prepared from a $CuSO_4{\cdot}5H_2O$ salt and Cu^{I} from a $Cu(CH_3CN)_4BF_4$ salt first dissolved in acetonitrile at a concentration around 1 mM, the exact concentration was determined by adding excess sodium bicinchoninic acid (BCA, 2-(4-carboxyquinolin-2-yl)quinoline-4-carboxylic acid) and measuring the absorbance of $Cu(BCA)_2^{3-}$ with an extinction coefficient of 7700 $M^{-1}cm^{-1}$ at 562 nm. When noted, the Cu^{I} was generated in situ by the reduction of Cu^{II} with ascorbate for the ROS experiments or dithionite for the NMR experiments.

HEPES buffer (sodium salt of 2-[4-(2-hydroxyethyl)piperazin-1-yl]ethanesulfonic acid) was prepared at an initial concentration of 500 mM, pH 7.4. Phosphate buffer, K_2HPO_4 and KH_2PO_4, were prepared at 500 mM, and they were mixed to reach a stock solution at 500 mM, pH 7.4. Sodium ascorbate was prepared at 5 mM and freshly used. Cu(peptides) complexes were prepared in situ by the mixing of the appropriate quantity of peptide stock solutions (ca. 1 mM) and $CuSO_4$ stock solution (ca. 1 mM) in a buffer (see figure captions for more details). Ferrozine was prepared at 20 mM, pH 7.4, and titrated with the Cu^{I} solution to determine the exact Fz concentration.

Peptides $A\beta_{1-16}$, $A\beta_{4-16}$ and $A\beta_{11-16}$ (DAEFRHDSGYEVHHQK, FRHDSGYEVHHQK and EVHHQK respectively) were purchased from Genecust. Stock solutions were prepared at around 10 mM and stored at 4 °C. For Tyr containing peptide, concentration was determined by UV ($\varepsilon_{276-296} = 1410\ cm^{-1}M^{-1}$ at acidic pH). For the *N*-truncated peptides, the exact concentration was determined by a Cu^{II} titration following the appearance of the d-d transition by UV/Vis at the maximum absorption ($\lambda = 520$ nm).

UV/Vis spectra were recorded with a Hewlett Packard Agilent 8453 spectrophotometer at 25 °C with an 800 rpm stirring.

Affinity for Cu^{I}: The apparent affinity constants at pH 7.4 of the Cu^{I} complexes ($Cu^{I}(A\beta_{1-16})$, $Cu^{I}(A\beta_{4-16})$ and $Cu^{I}(A\beta_{11-16})$) were measured by UV/Vis titrations in the presence of ferrozine (Fz) as a competitor in a 1 cm path length sealed quartz cuvettes under argon, with 800 rpm stirring. All the solution were prepared in Ar-degassed HEPES. The $Cu(Fz)_2^{3-}$ complex (55 μM) in HEPES (100 mM, pH 7.4) was first formed in situ, the different peptides were then added (ca. 100 μM per addition). The spectra were recorded and show the decrease of the 470 nm absorption band characteristic of the $Cu(Fz)_2^{3-}$ complex (with a molar extinction coefficient value $\varepsilon = 4320\ M^{-1}cm^{-1}$). The $Cu^{I}(A\beta_{n-16})$ association constants were then determined using the binding constant of the $Cu(Fz)_2^{3-}$ ($\log\beta_{12} = 11.6$) described in the literature.

Electron paramagnetic resonance: Electron paramagnetic resonance (EPR) data were recorded with an Elexsys E 500 Bruker spectrometer, operating at a microwave frequency of approximately 9.5 GHz. Spectra were recorded using a microwave power of 2 mW

across a sweep width of 150 mT (centred at 310 mT) with modulation amplitude of 0.5 mT. Experiments were carried out at 110 K using a liquid nitrogen cryostat.

EPR samples were prepared from stock solution of peptides diluted to 0.2 mM in H_2O. ^{65}Cu(II) (0.9 equiv.) was added from $^{65}Cu(NO_3)_2$ (78 mM) stock solution made in-house from ^{65}Cu foil. If necessary, pH was adjusted to 7.4 with H_2SO_4 and NaOH solutions. Samples were frozen in a quartz tube after addition of 10% glycerol as a cryoprotectant and stored in liquid nitrogen until used.

Electrochemical experiments: Electrochemical experiments were performed in an argon-flushed cell. A three-electrode setup was used, consisting of a glassy carbon (3 mm in diameter) disk as a working electrode, a platinum wire auxiliary electrode and a Saturated Calomel Electrode as reference electrode directly dipped into the solution. Cyclic voltammograms were recorded with an Autolab PGSTAT302N potentiostat piloted by EC-Lab software. The working electrode was carefully polished before each measurement on a red disk NAP with 1 μm AP-A suspension during at least one minute (Struers). Additional support electrolyte was not added because of the high concentration of phosphate buffer in the solution. The scanning speed was 0.1 $V.s^{-1}$. The samples were prepared from stock solutions of peptides and Cu^{II} diluted to the desired concentration.

Stopped-flow measurements: Rapid-mixing UV/Vis spectroscopy was carried out using a SFM-20 two syringes stopped-flow system from Biologic combined with a diode array spectrometer composed of a TIDAS J&M MMS-UV/VIS 500-3 detector and a light source HAMAMATSU L7893 incorporating deuterium and tungsten lamps with optical fibres. Data acquisition, extraction and treatment were realized with the Bio-Kine software. The syringes (Hamilton) are mounted on a rigid drive platform ensuring that the flow was stopped precisely and instantaneously. The content of the two syringes were rapidly mixed in the mixing chamber and the absorbance of the system was recorded over time as full spectra after designated time delays. Typically, for the Cu^{II} binding affinity, one syringe was filled with a solution of peptide at 0.1 mM in HEPES buffer (200 mM, pH 7.4), and the second was filled with a solution of $CuSO_4$ in water at 0.08 mM. An equal quantity of the two solutions were mixed to reach a final concentration of Cu^{II} of 416.5 μM and peptide of 500 μM in HEPES buffer (100 mM, pH 7.4). The $t_{1/2}$ was evaluated as the time required to performed half of the reaction; i.e., the time required to reach half of the maximum absorbance value at 520 nm.

NMR: The ^1H NMR experiments were recorded with a Bruker Avance NEO 600 spectrometer equipped with a 5 mm broadband inverse triple-resonance probe ^1H, BB (^{31}P-^{103}Rh)/^{31}P with Z field gradients. The presaturation of the water signal was achieved with a zqpr sequence (Bruker). ^1H NMR experiments were performed at 298 K. The peptides were dissolved in D_2O and the concentration was determined as previously described. All the manipulations described below were performed under Ar, with Ar-degassed solutions. 2 equiv (per Cu ion) of a 100 mM freshly prepared dithionite solution in D_2O were added with a syringe to a $CuSO_4$ solution in a 200 mM phosphate buffer in D_2O. 1 equiv (per peptide) of the resulting Cu^I-containing solution was immediately added to a degassed solution of peptide (Ar for 20 min). The resulting Cu^I complex at 0.5 mM was then introduced by using a syringe in an Ar-degassed NMR tube and sealed.

ROS formation: Ascorbate consumption was monitored by UV/Vis spectrophotometry. The decrease of the absorption band at $\lambda_{max}=$ 265 nm of the Asc ($\varepsilon = 14500\ M^{-1}cm^{-1}$, corrected at 800 nm) was plotted as a function of time. The samples were prepared from stock solutions of peptides and Cu^{II} diluted to 12 and 10 μM, respectively, in HEPES (100 mM, pH 7.4) in a 1 cm or a 2 mm path length quartz cuvette. In the competition experiments, both peptides ($A\beta_{1-16}$ and $A\beta_{4/11-16}$) were at 12 μM. Ascorbate was added to obtain 100 μM or 500 μM as the final concentration. Final volume was adjusted with milliQ water to 2 mL.

Acknowledgements

The authors thank the ERC aLzINK—Contract no. 638712 for financial support. CE thanks the PRESTIGE Programm (grant no. PCOFUND-GA-2013–609102). The authors acknowledge Christian Bijani for the recording of the ^1H NMR spectra. Drs. Amandine Conte-Daban, Mireia Tomas I Giner, and Laurent Sabater are gratefully acknowledged for their contributions and Dr. Karine Reybier for access to the EPR facility.

Conflict of interest

The authors declare no conflict of interest.

Keywords: amyloid beta-peptides · bioinorganic chemistry · chelates · copper · reactive oxygen species

[1] J. Hardy, G. Higgins, *Science* **1992**, *256*, 184–185.
[2] a) E. Portelius, N. Bogdanovic, M. K. Gustavsson, I. Volkmann, G. Brinkmalm, H. Zetterberg, B. Winblad, K. Blennow, *Acta Neuropathol.* **2010**, *120*, 185–193; b) C. L. Masters, G. Simms, N. A. Weinman, G. Multhaup, B. L. McDonald, K. Beyreuther, *Proc. Natl. Acad. Sci. USA* **1985**, *82*, 4245.
[3] a) K. Liu, I. Solano, D. Mann, C. Lemere, M. Mercken, J. Q. Trojanowski, V. M. Y. Lee, *Acta Neuropathol.* **2006**, *112*, 163–174; b) V. Borghesani, B. Alies, C. Hureau, *Eur. J. Inorg. Chem.* **2018**, 7–15; c) M. P. Kummer, M. T. Heneka, *Alzheimers Res. Ther.* **2014**, *6*, 28; d) V. Lanza, F. Bellia, E. Rizzarelli, *Coord. Chem. Rev.* **2018**, *369*, 1–14.
[4] S. Z. O. Wirths, S. Weggen in *Alzheimer's Disease [Internet]* (Ed.: Ed.: T. Wisniewski), Codon Publications, Brisbane, **2019**, pp. 107–122.
[5] J. Naslund, A. Schierhorn, U. Hellman, L. Lannfelt, A. D. Roses, L. O. Tjernberg, J. Silberring, S. E. Gandy, B. Winblad, P. Greengard, *Proc. Natl. Acad. Sci. USA* **1994**, *91*, 8378.
[6] Y. M. Kuo, T. A. Kokjohn, T. G. Beach, L. I. Sue, D. Brune, J. C. Lopez, W. M. Kalback, D. Abramowski, C. Sturchler-Pierrat, M. Staufenbiel, A. E. Roher, *J. Biol. Chem.* **2001**, *276*, 12991–12998.
[7] a) E. Stefaniak, W. Bal, *Inorg. Chem.* **2019**, *58*, 13561–13577; b) P. Gonzalez, K. Bossak, E. Stefaniak, C. Hureau, L. Raibaut, W. Bal, P. Faller, *Chem. Eur. J.* **2018**, *24*, 8029–8041; c) S. C. Drew, *Front. Neurosci.* **2017**, *11*, 317.
[8] C. Hureau, *Encyclopedia of Inorganic and Bioinorganic Chemistry* (Ed.: R. A. Scott), John Wiley & Sons, Ltd., Hoboken, **2019**, pp. 1–14.
[9] a) V. Balland, C. Hureau, J.-M. Savéant, *Proc. Natl. Acad. Sci. USA* **2010**, *107*, 17113–17118; b) C. Hureau, V. Balland, Y. Coppel, P. L. Solari, E. Fonda, P. Faller, *J. Biol. Inorg. Chem.* **2009**, *14*, 995–1000; c) C. Hureau, P. Faller, *Biochimie* **2009**, *91*, 1212–1217; d) L. G. Trujano-Ortiz, F. J. González, L. Quintanar, *Inorg. Chem.* **2015**, *54*, 4–6; e) C. Cheignon, M. Jones, E. Atrián-Blasco, I. Kieffer, P. Faller, F. Collin, C. Hureau, *Chem. Sci.* **2017**, *8*, 5107–5118.
[10] C. Hureau, *Coord. Chem. Rev.* **2012**, *256*, 2164–2174.
[11] a) E. Atrián-Blasco, P. Gonzalez, A. Santoro, B. Alies, P. Faller, C. Hureau, *Coord. Chem. Rev.* **2018**, *371*, 38–55; b) S. C. Drew, K. J. Barnham, *Acc. Chem. Res.* **2011**, *44*, 1146–1155; c) C. Hureau, P. Dorlet, *Coord. Chem. Rev.* **2012**, *256*, 2175–2187.
[12] a) B. Alies, E. Renaglia, M. Rózga, W. Bal, P. Faller, C. Hureau, *Anal. Chem.* **2013**, *85*, 1501–1508; b) A. Conte-Daban, V. Borghesani, S. Sayen, E. Guillon, Y. Journaux, G. Gontard, L. Lisnard, C. Hureau, *Anal. Chem.* **2017**, *89*, 2155–2162.
[13] a) M. Mital, N. E. Wezynfeld, T. Frączyk, M. Z. Wiloch, U. E. Wawrzyniak, A. Bonna, C. Tumpach, K. J. Barnham, C. L. Haigh, W. Bal, S. C. Drew,

Angew. Chem. Int. Ed. **2015**, *54*, 10460 – 10464; *Angew. Chem.* **2015**, *127*, 10606 – 10610; b) J. D. Barritt, J. H. Viles, *J. Biol. Chem.* **2015**, *290*, 27791 – 27802.
[14] T. Kowalik-Jankowska, M. Ruta-Dolejsz, K. Wiśniewska, L. Łankiewicz, H. Kozłowski, *J. Chem. Soc. Dalton Trans.* **2000**, 4511 – 4519.
[15] a) G. De Gregorio, F. Biasotto, A. Hecel, M. Luczkowski, H. Kozlowski, D. Valensin, *J. Inorg. Biochem.* **2019**, *195*, 31 – 38; b) J. Shearer, V. A. Szalai, *J. Am. Chem. Soc.* **2008**, *130*, 17826 – 17835.
[16] a) T. R. Young, A. Kirchner, A. G. Wedd, Z. Xiao, *Metallomics* **2014**, *6*, 505 – 517; b) B. Alies, B. Badei, P. Faller, C. Hureau, *Chem. Eur. J.* **2012**, *18*, 1161 – 1167; c) Z. Xiao, L. Gottschlich, R. van der Meulen, S. R. Udagedara, A. G. Wedd, *Metallomics* **2013**, *5*, 501 – 513.
[17] E. Atrián-Blasco, M. del Barrio, P. Faller, C. Hureau, *Anal. Chem.* **2018**, *90*, 5909 – 5915.
[18] F. Arrigoni, T. Prosdocimi, L. Mollica, L. De Gioia, G. Zampella, L. Bertini, *Metallomics* **2018**, *10*, 1618 – 1630.
[19] a) M. J. Pushie, E. Stefaniak, M. R. Sendzik, D. Sokaras, T. Kroll, K. L. Haas, *Inorg. Chem.* **2019**, *58*, 15138 – 15154; b) V. A. Streltsov, R. S. K. Ekanayake, S. C. Drew, C. T. Chantler, S. P. Best, *Inorg. Chem.* **2018**, *57*, 11422 – 11435.
[20] N. E. Wezynfeld, E. Stefaniak, K. Stachucy, A. Drozd, D. Płonka, S. C. Drew, A. Krężel, W. Bal, *Angew. Chem. Int. Ed.* **2016**, *55*, 8235 – 8238; *Angew. Chem.* **2016**, *128*, 8375 – 8378.
[21] X. Teng, E. Stefaniak, P. Girvan, R. Kotuniak, D. Płonka, W. Bal, L. Ying, *Metallomics* **2020**, *12*, 470 – 473.
[22] R. Kotuniak, M. J. F. Strampraad, K. Bossak-Ahmad, U. E. Wawrzyniak, I. Ufnalska, P.-L. Hagedoorn, W. Bal, *Angew. Chem. Int. Ed.* **2020**, *59*, 11234 – 11239; *Angew. Chem.* **2020**, *132*, 11330 – 11335.
[23] a) S. E. Conklin, E. C. Bridgman, Q. Su, P. Riggs-Gelasco, K. L. Haas, K. J. Franz, *Biochemistry* **2017**, *56*, 4244 – 4255; b) K. L. Haas, A. B. Putterman, D. R. White, D. J. Thiele, K. J. Franz, *J. Am. Chem. Soc.* **2011**, *133*, 4427 – 4437.
[24] P. Gonzalez, K. Bossak-Ahmad, B. Vileno, N. E. Wezynfeld, Y. El Khoury, P. Hellwig, C. Hureau, W. Bal, P. Faller, *Chem. Commun.* **2019**, *55*, 8110 – 8113.
[25] J. W. Karr, H. Akintoye, L. J. Kaupp, V. A. Szalai, *Biochemistry* **2005**, *44*, 5478 – 5487.
[26] T. A. Enache, A. M. Oliveira-Brett, *J. Electroanal. Chem.* **2011**, *655*, 9 – 16.
[27] M. Z. Wiloch, I. Ufnalska, A. Bonna, W. Bal, W. Wróblewski, U. E. Wawrzyniak, *J. Electrochem. Soc.* **2017**, *164*, G77 – G81.
[28] a) P. Gonzalez, B. Vileno, K. Bossak, Y. El Khoury, P. Hellwig, W. Bal, C. Hureau, P. Faller, *Inorg. Chem.* **2017**, *56*, 14870 – 14879; b) C. Hureau, H. Eury, R. Guillot, C. Bijani, S. Sayen, P.-L. Solari, E. Guillon, P. Faller, P. Dorlet, *Chem. Eur. J.* **2011**, *17*, 10151 – 10160.
[29] N. E. Wezynfeld, A. Tobolska, M. Mital, U. E. Wawrzyniak, M. Z. Wiloch, D. Płonka, K. Bossak-Ahmad, W. Wróblewski, W. Bal, *Inorg. Chem.* **2020**, *59*, 14000 – 14011.
[30] a) B. Alies, C. Bijani, S. Sayen, E. Guillon, P. Faller, C. Hureau, *Inorg. Chem.* **2012**, *51*, 12988 – 13000; b) H. Eury, C. Bijani, P. Faller, C. Hureau, *Angew. Chem. Int. Ed.* **2011**, *50*, 901 – 905; *Angew. Chem.* **2011**, *123*, 931 – 935; c) A. Jancsó, K. Selmeczi, P. Gizzi, N. V. Nagy, T. Gajda, B. Henry, *J. Inorg. Biochem.* **2011**, *105*, 92 – 101; d) C. Livera, L. D. Pettit, M. Bataille, J. Krembel, W. Bal, H. Kozlowski, *J. Chem. Soc. Dalton Trans.* **1988**, 1357 – 1360.
[31] A. Conte-Daban, B. Boff, A. Candido, C. Montes Aparicio, C. Gateau, C. Lebrun, G. Cerchiaro, I. Kieffer, S. Sayen, E. Guillon, P. Delangle, C. Hureau, *Chem. Eur. J.* **2017**, *23*, 17078 – 17088.
[32] a) S. Chassaing, F. Collin, P. Dorlet, J. Gout, C. Hureau, P. Faller, *Curr. Top. Med. Chem.* **2012**, *12*, 2573 – 2595; b) B. Alies, I. Sasaki, O. Proux, S. Sayen, E. Guillon, P. Faller, C. Hureau, *Chem. Commun.* **2013**, *49*, 1214 – 1216.
[33] A. Conte-Daban, A. Day, P. Faller, C. Hureau, *Dalton Trans.* **2016**, *45*, 15671 – 15678.
[34] a) R. Figueroa-Méndez, S. Rivas-Arancibia, *Front. Physiol.* **2015**, *6*; b) A. Carreau, B. E. Hafny-Rahbi, A. Matejuk, C. Grillon, C. Kieda, *J. Cell. Mol. Med.* **2011**, *15*, 1239 – 1253.
[35] F. E. Harrison, J. M. May, *Free Radic. Biol. Med.* **2009**, *46*, 719 – 730.
[36] a) C. Cheignon, P. Faller, D. Testemale, C. Hureau, F. Collin, *Metallomics* **2016**, *8*, 1081 – 1089; b) L.-E. Cassagnes, V. Hervé, F. Nepveu, C. Hureau, P. Faller, F. Collin, *Angew. Chem. Int. Ed.* **2013**, *52*, 11110 – 11113; *Angew. Chem.* **2013**, *125*, 11316 – 11319.
[37] D. S. Folk, K. J. Franz, *J. Am. Chem. Soc.* **2010**, *132*, 4994 – 4995.
[38] a) A. B. Caballero, L. Terol-Ordaz, A. Espargaró, G. Vázquez, E. Nicolás, R. Sabaté, P. Gamez, *Chem. Eur. J.* **2016**, *22*, 7268 – 7280; b) X. Hu, Q. Zhang, W. Wang, Z. Yuan, X. Zhu, B. Chen, X. Chen, *ACS Chem. Neurosci.* **2016**, *7*, 1255 – 1263.
[39] C. Esmieu, D. Guettas, A. Conte-Daban, L. Sabater, P. Faller, C. Hureau, *Inorg. Chem.* **2019**, *58*, 13509 – 13527.

Manuscript received: August 27, 2020
Revised manuscript received: October 7, 2020
Accepted manuscript online: October 15, 2020
Version of record online: December 14, 2020